NASA TECHNICAL NOTE

NASA TN D-3320

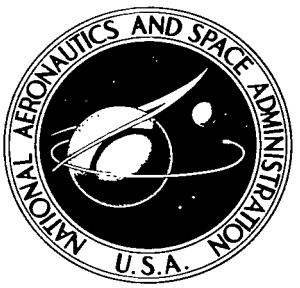

NASA TN D-3320

LONGITUDINAL AERODYNAMIC CHARACTERISTICS OF TWO BLUNTED CONE REENTRY CONFIGURATIONS AT MACH NUMBERS FROM 17.6 TO 22.2 INCLUDING SOME REYNOLDS NUMBER EFFECTS

by Dal V. Maddalon

Langley Research Center
Langley Station, Hampton, Va.

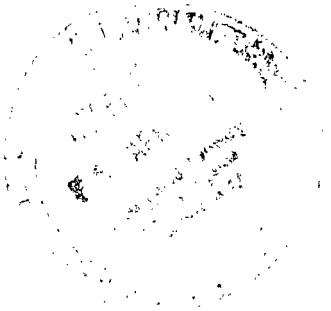

NATIONAL AERONAUTICS AND SPACE ADMINISTRATION • WASHINGTON, D. C. • MARCH 1966

NASA TN D-3320

LONGITUDINAL AERODYNAMIC CHARACTERISTICS OF TWO BLUNTED CONE REENTRY CONFIGURATIONS AT MACH NUMBERS FROM 17.6 TO 22.2 INCLUDING SOME REYNOLDS NUMBER EFFECTS

By Dal V. Maddalon

Langley Research Center
Langley Station, Hampton, Va.

NATIONAL AERONAUTICS AND SPACE ADMINISTRATION

For sale by the Clearinghouse for Federal Scientific and Technical Information
Springfield, Virginia 22151 – Price $0.45

LONGITUDINAL AERODYNAMIC CHARACTERISTICS OF TWO BLUNTED CONE REENTRY CONFIGURATIONS AT MACH NUMBERS FROM 17.6 TO 22.2 INCLUDING SOME REYNOLDS NUMBER EFFECTS

By Dal V. Maddalon
Langley Research Center

SUMMARY

The longitudinal aerodynamic characteristics of two reentry vehicles (a blunted cone and a blunted cylinder-cone) have been obtained at Mach numbers from 17.6 to 22.2 and Reynolds numbers (based on maximum body diameter) from 0.12×10^6 to 3.76×10^6. Contrary to results from a previous study on the blunted cylinder-cone configuration, the center-of-pressure location was found to be essentially independent of Reynolds number. In addition, the zero-angle-of-attack drag coefficient of the blunted cone reentry body was independent of Reynolds number whereas some viscous effects existed on the blunted cylinder-cone configuration.

INTRODUCTION

The blunted cone has recently received a good deal of attention from both theoretical and experimental aerodynamicists as a result of its very favorable heating performance in ballistic and reentry flight programs. One application of this configuration is a reentry body investigated in this study and denoted herein as the R-5 reentry configuration. (The configuration is not currently being considered for an actual flight test.)

When the high Mach number wind-tunnel investigation on this body was initiated it was decided to obtain the aerodynamic characteristics over a considerable range of Reynolds number as a result of previous work on a similar reentry configuration that indicated that center-of-pressure location (ref. 1) and pitching-moment coefficient (ref. 2) were dependent on Reynolds number. This earlier model (designated in ref. 1 and in this study as N_4B_4) can be described as having a spherically segmented nose followed by a short

cylindrical section and a 9° half-angle cone body with a truncated conical base. In contrast, the R-5 configuration has a blunter nose followed by a corner radius and a 9° half-angle cone body (see fig. 1 for a comparative sketch of these two configurations). The results of the tests on the R-5 configuration led to a reexamination of the N_4B_4 configuration.

Tests were conducted at Mach numbers from 17.6 to 22.2 and Reynolds numbers (based on maximum body diameter) from 0.12×10^6 to 3.76×10^6.

SYMBOLS

Measurements for this investigation were taken in the U.S. Customary Units but are also given parenthetically in the International System of Units (SI) to encourage its use in future NASA reports. Historical information, physical constants, and conversion factors of the International System are included in reference 3. Conversion factors pertinent to the present investigation are as follows:

Physical quantity	U.S. Customary Unit	Conversion factor (*)	SI unit
Length	in.	2.54	centimeter (cm)
	ft	0.3048	meter (m)
Pressure	psia	6894.7572	newtons/meter^2 (N/m^2)
Temperature . . .	°R	5/9	degrees Kelvin (°K)

*Multiply value given in U.S. Customary Unit by conversion factor to obtain equivalent value in SI unit.

C_A axial-force coefficient, $\frac{\text{Axial force}}{qS}$

C_D drag coefficient, $\frac{\text{Drag force}}{qS}$

C_m pitching-moment coefficient, $\frac{\text{Pitching moment}}{qSD}$

$C_{m_\alpha} = \left(\frac{\partial C_m}{\partial \alpha}\right)_{\alpha=0^\circ}$

C_N normal-force coefficient, $\frac{\text{Normal force}}{qS}$

$C_{N_\alpha} = \left(\frac{\partial C_N}{\partial \alpha}\right)_{\alpha=0^\circ}$

C_p pressure coefficient

D maximum body diameter, in. or cm (see fig. 1)

M free-stream Mach number

q free-stream dynamic pressure, lb/in^2 or N/cm^2

R_D free-stream Reynolds number (based on maximum body diameter)

S base area, in^2 or cm^2 (based on maximum body diameter)

x_{cm} distance from nose to moment reference position, in. or cm

$\frac{x_{cp}}{D} = \left[\frac{x_{cm}}{D} - \left(\frac{\partial C_m}{\partial C_N}\right)_{\alpha=0^\circ}\right]$ center-of-pressure location, measured from nose and referenced to maximum body diameter

α angle of attack, deg

γ ratio of specific heats

Subscripts:

$\alpha=0^\circ$ parameter at zero-degree angle of attack

max maximum

APPARATUS AND TESTS

Models

In order to obtain a wide range of Reynolds number, the model dimensions as well as the pressure in the tunnel stagnation chamber were varied. The pertinent dimensions of each model can be obtained by using the scale size listed in table I together with the appropriate sketch of figure 1.

All models were fabricated from aluminum and had their external surfaces highly polished.

Facility and Instrumentation

Tests were conducted by utilizing a contoured nozzle in the Langley 22-inch helium tunnel. A comprehensive calibration and a description of this tunnel may be found in reference 4. A cutaway perspective of this facility with the contoured nozzle is presented in figure 2. During the present investigation, the range of temperatures encountered in the tunnel stagnation chamber was approximately 515° R (286° K) to 550° R (306° K) while the total pressure varied from 213 psia $\left(1.47 \times 10^6 \text{ N/m}^2\right)$ to 3023 psia $\left(20.84 \times 10^6 \text{ N/m}^2\right)$. Increasing the reservoir pressure in this manner thinned the boundary layer on the tunnel wall, and the test-section Mach number therefore varied from 17.6 to 22.2. Values of Mach number are accurate to approximately ±1 percent. The flow angularity existing in this nozzle was investigated in reference 4 at several stagnation pressures and was negligible within the accuracy of the calibration.

Because of the large variation in anticipated loads, several sting-mounted strain-gage balances were used to measure the static longitudinal forces and moments. The maximum inaccuracies in the aerodynamic coefficients as determined from static balance calibrations are listed in table II.

Description of Tests

Most tests were conducted through angles of attack ranging from -4° to +18°. In the course of the test, the model made a continuous traverse of the angle-of-attack range by means of a sting mechanism hydraulically operated at a speed of about 3 deg/sec. A prism mounted rearward of the model base reflected light from a source onto a steel plate on which were set a number of small photoelectric cells at calibrated intervals. When a cell was energized, an electrical signal was sent to a high-speed digital recorder and the balance outputs were sampled and recorded. In addition, the model traveled through the angle-of-attack range twice (once in each direction) to compensate for the physical size of the photoelectric cell. Therefore, two slightly different data points were obtained at each angle of attack. The data shown in this report represent the average of the two groups of data. No base pressure corrections were made to the data.

Theoretical Calculations

Results obtained by Newtonian theory have been compared with the data generated in this investigation. Coefficients were computed by the method of reference 5 with a correction added to account for the pitching moment caused by axial force. The value of $C_{p,max}$ used in these calculations was determined to be 1.75 by the following equation from reference 6:

$$C_{p,max} = \frac{\gamma + 3}{\gamma + 1}\left[1 - \frac{2}{(\gamma + 3)M^2}\right]$$

Because $C_{p,max}$ has been corrected in this manner, all references to theoretical values in this study are denoted as modified Newtonian theory.

RESULTS AND DISCUSSION

In the following discussion, all force and moment coefficients are referenced to the maximum body area and maximum body diameter. The reference points for the pitching-moment coefficients are 0.760D and 0.766D rearward of the nose for the R-5 and the N_4B_4 configurations, respectively.

R-5 Reentry Configuration

The basic data for the R-5 reentry configuration are shown in figure 3 at various test Mach numbers and Reynolds numbers. The aerodynamic coefficients are presented with varying Reynolds number in figure 4 where no significant viscous effect is discernible within the accuracy of the data. Comparison between the theoretical prediction for normal-force coefficient and the experimental results shows theory to overestimate the experimental data for all angles of attack. Axial-force coefficient disagreed with theory by approximately 10 percent at low angles of attack but the agreement generally improved with increased angle of attack. Close agreement between theory and experiment was obtained at the maximum angles of the investigation. The normal-force-curve slope as a function of Reynolds number is shown in figure 5. This coefficient is apparently insensitive to varying Reynolds number and is considerably overestimated by the Newtonian theory. In figure 6 is shown the slope of the pitching-moment curve which is also essentially constant with varying Reynolds number. For this parameter, however, the theory underestimates the data. Figure 7 presents both the modified Newtonian prediction and the experimental center-of-pressure results with varying Reynolds number. It is evident that viscous forces do not affect this parameter within the Reynolds number range investigated.

N_4B_4 Reentry Configuration

The unexpected difference in the behavior of the center-of-pressure location (with regard to Reynolds number) between the R-5 configuration results of the present investigation and the N_4B_4 configuration results of reference 1 led to a reexamination of the aerodynamic characteristics of the N_4B_4 configuration. Additional tests were conducted for several different Reynolds numbers and the basic data from these tests are plotted in figure 8 together with the modified Newtonian predictions. The center-of-pressure results are presented in figure 9 along with the previous data of reference 1. Note that the center-of-pressure location for the present tests is essentially constant with varying Reynolds number. This discrepancy between the original results and the present data is

attributed to differences in test-section flow conditions. Lateral variations in Mach number from the average test-core Mach number, which were thought to be of little consequence at the time the tests of reference 1 were conducted, were later found to be of significance. The nozzle was then remachined and the quality of the flow was improved to the extent that lateral variations in test-core Mach number were reduced to about one-half of that during the previous tests (Mach number surveys in the remachined nozzle are contained in ref. 4). As a lateral Mach number deviation would be affected by variation in Reynolds number through its effect on tunnel-wall boundary-layer thickness, this deviation probably caused the Reynolds number effect on center-of-pressure location observed in reference 1. The present data are therefore thought to be more nearly correct than the previous data. No explanation is available for the wide deviation in center-of-pressure location which exists between the present data and that from tests at comparable Mach numbers in several other facilities.

Additional measurements of $C_{D,\alpha=0^\circ}$ for the N_4B_4 configuration at various Reynolds numbers are shown in figure 10 along with data for the R-5 configuration. Also included in this figure are results from oil flow studies (photographs of which are presented in fig. 11) which indicate the Reynolds number for flow detachment. From this plot it is evident that significant variations in the $\alpha = 0^\circ$ drag coefficient occur on the N_4B_4 configuration as the Reynolds number varies. A meaningful explanation of the low drag-coefficient region existing between $R_D = 0.24 \times 10^6$ and $R_D = 2.37 \times 10^6$ would require detailed pressure and heat-transfer measurements on the model's surface and base. As these measurements were beyond the scope of the present investigation, no analysis will be attempted. It is noted, however, that reference 7 at $M \approx 24$ indicated that the induced pressure distribution at $\alpha = 0^\circ$ on cylindrical bodies depends to some extent on Reynolds number (especially in the region of the nose-cylinder junction), and the N_4B_4 configuration is essentially cylindrical over the initial portion of its length. In view of the preceding observations regarding viscous effects on pressure distribution and drag at $\alpha = 0^\circ$, the small amount of theoretical and experimental information available concerning these effects on blunt bodies is rather surprising and would seem to warrant further investigation.

Photographs of the various flow patterns taken during the tests at zero angle of attack are presented in figure 11. These results show that, although the flow was attached at the lower Reynolds numbers, separation did occur at $R_D \approx 0.53 \times 10^6$. This value, however, is well within the region of reduced $C_{D,\alpha=0^\circ}$ (see fig. 10) and, therefore, it appears that the detached-flow condition is not solely responsible for the lower drag coefficient values. In an attempt to gain some insight into the effect of varying angle of attack at different Reynolds numbers, additional oil flow tests were conducted at $\alpha = 2^\circ$, $R_D = 0.27 \times 10^6$, and at $\alpha = 4^\circ$, $R_D = 2.35 \times 10^6$. Photographs of these tests are shown in fig. 12. Although these two tests are for dissimilar angles of attack, it is considered significant that the differences in local flow characteristics noted at $\alpha = 0^\circ$ (with respect to Reynolds number) are still present at these angles of attack in that the flow remained attached for the low Reynolds number and remained separated for the high Reynolds number. It might

therefore be expected that these phenomena would be evident in pitching-moment coefficient and, therefore, in center-of-pressure position. As mentioned earlier, however, no such result was observed to any significant degree.

Comparison of Configurations

The differences in the variation of the $\alpha = 0^\circ$ drag coefficient with Reynolds number (see fig. 10) between the N_4B_4 and the R-5 configurations are not fully understood at this time. Possible explanations must consider the differences in configuration design, the most basic of which are nose corner geometry, fineness ratio, nose bluntness, and the cylindrical section forward of the cone body on the N_4B_4 configuration. Of the four, this cylindrical section is probably the most important as it is followed by a 9° conical afterbody which causes the boundary layer to separate for sufficiently high Reynolds number. This type of viscous effect, which occurs very close to the nose of the N_4B_4 configuration, can influence the flow over a large portion of the body and, therefore, the fineness ratio of the model becomes important. In the extreme case of a model with a very low fineness ratio, viscous effects might dominate the entire flow field, whereas for a model with a high fineness ratio the effects would be concentrated in the region near the cylinder-cone junction and would be relatively insignificant for the configuration as a whole. In regard to the effect of bluntness on the pressures in the region of the junction, reference 7 has indicated that the effects of Reynolds number on the induced pressures of blunt cylinders are small for high-nose-drag cylinders.

CONCLUDING REMARKS

The longitudinal aerodynamic characteristics of two reentry configurations (a blunted cone and a blunted cylinder-cone) have been obtained at Mach numbers from 17.6 to 22.2 for a wide range of Reynolds numbers. The center-of-pressure position on both configurations was found to be essentially constant with varying Reynolds number, a phenomenon contrary to the results of NASA TN D-1638, which contains an earlier study of one of the two configurations investigated. Significant Reynolds number effects, however, were present for the zero-angle-of-attack drag coefficient of the blunted cylinder-cone configuration whereas no viscous effects were apparent on the blunted cone configuration. Analysis of this discrepancy was limited by the general lack of knowledge concerning viscous effects on blunt bodies at high Mach numbers.

Langley Research Center,
National Aeronautics and Space Administration,
Langley Station, Hampton, Va., July 9, 1965.

REFERENCES

1. Johnston, Patrick J.: Longitudinal Aerodynamic Characteristics of Several Fifth-Stage Scout Reentry Vehicles From Mach Number 0.60 to 24.4 Including Some Reynolds Number Effects on Stability at Hypersonic Speeds. NASA TN D-1638, 1963.

2. Pope, T. C.: Additional Force Data Obtained in the Chance Vought Hypervelocity Wind Tunnel on a Five Stage Scout Payload Re-Entry Configuration at a Mach Number of 17. Rept. No. HVWT Test 13F, Aeron. and Missiles Div., Chance Vought Corp., June 21, 1963.

3. Mechtly, E. A.: The International System of Units - Physical Constants and Conversion Factors. NASA SP-7012, 1964.

4. Arrington, James P.; Joiner, Roy C., Jr.; and Henderson, Arthur, Jr.: Longitudinal Characteristics of Several Configurations at Hypersonic Mach Numbers in Conical and Contoured Nozzles. NASA TN D-2489, 1964.

5. Rainey, Robert W.: Working Charts for Rapid Prediction of Force and Pressure Coefficients on Arbitrary Bodies of Revolution by Use of Newtonian Concepts. NASA TN D-176, 1959.

6. Lees, Lester: Hypersonic Flow. Fifth Intern. Aeron. Conf. (Los Angeles, Calif.), Inst. Aeron. Sci., Inc., June 1955, pp. 241-276.

7. Wagner, Richard D., Jr.; and Watson, Ralph: Reynolds Number Effects on the Induced Pressures of Cylindrical Bodies With Different Nose Shapes and Nose Drag Coefficients in Helium at a Mach Number of 24. NASA TR R-182, 1963.

TABLE I.- REFERENCE DIMENSIONS AND TEST CONDITIONS

Scale	D, in.	(cm)	S, in^2	(cm^2)	R_D	M
R-5 reentry configuration (full scale D of 14.06 in. (35.712 cm))						
1/12	1.173	(2.979)	1.081	(6.974)	0.25×10^6	19.0
1/8	1.757	(4.463)	2.425	(15.645)	.38	19.0
1/8	1.757	(4.463)	2.425	(15.645)	.70	20.3
1/4	3.518	(8.936)	9.720	(62.710)	1.39	20.3
1/4	3.518	(8.936)	9.720	(62.710)	2.56	21.6
3/8	5.271	(13.388)	21.821	(140.780)	3.76	21.6
N_4B_4 reentry configuration (full scale D of 20.07 in. (50.975 cm))						
1/16	1.258	(3.195)	1.242	(8.013)	0.12×10^6	17.6
1/8	2.510	(6.375)	4.946	(31.910)	.24	17.6
1/16	1.258	(3.195)	1.242	(8.013)	.27	19.0
1/16	1.258	(3.195)	1.242	(8.013)	.36	19.8
1/8	2.510	(6.375)	4.946	(31.910)	.52	19.0
1/8	2.510	(6.375)	4.946	(31.910)	.72	19.8
1/8	2.510	(6.375)	4.946	(31.910)	.96	20.3
1/8	2.510	(6.375)	4.946	(31.910)	2.37	22.2
1/4	5.016	(12.741)	19.751	(127.426)	3.36	21.6

TABLE II.- BALANCE ACCURACY

R_D	Accuracy for:		
	C_N	C_A	C_m
R-5 reentry configuration			
0.25×10^6	±0.010	±0.019	±0.008
.38	±.004	±.008	±.002
.70	±.008	±.008	±.003
1.39	±.007	------	±.002
2.56	±.004	------	±.001
3.76	±.001	±.003	±.001
N_4B_4 reentry configuration			
0.12×10^6	------	±0.016	------
.24	------	±.004	------
.27	±0.002	±.008	±0.001
.36	------	±.006	------
.52	------	±.002	------
.72	------	±.002	------
.96	±.003	±.006	±.001
2.37	±.001	±.003	±.001
3.36	±.001	±.003	±.001

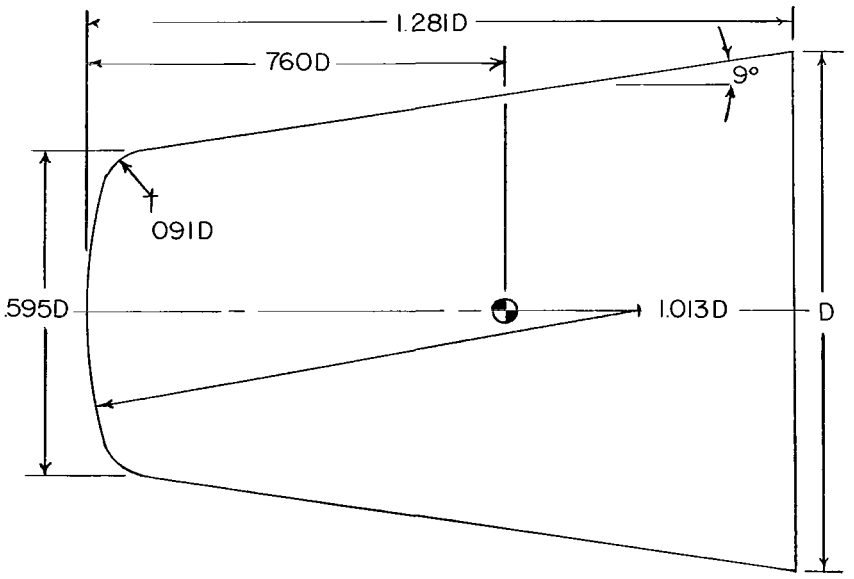

(a) R-5 reentry configuration.

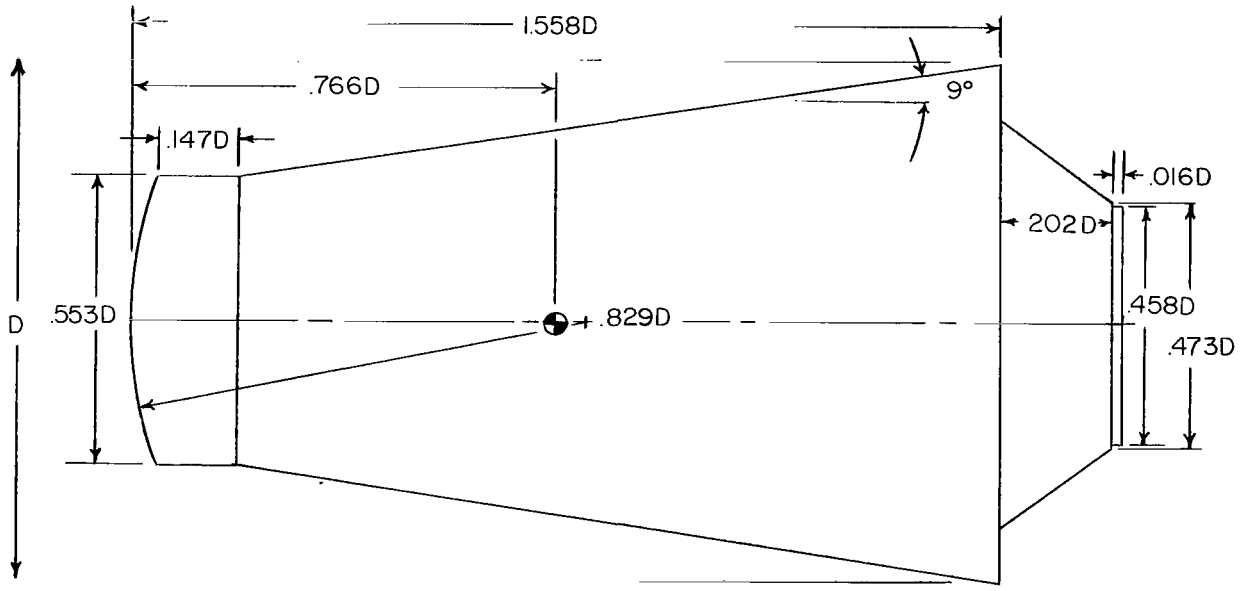

(b) N_4B_4 reentry configuration.

Figure 1.- Model dimensions in terms of reference diameters (see table I for values of D).

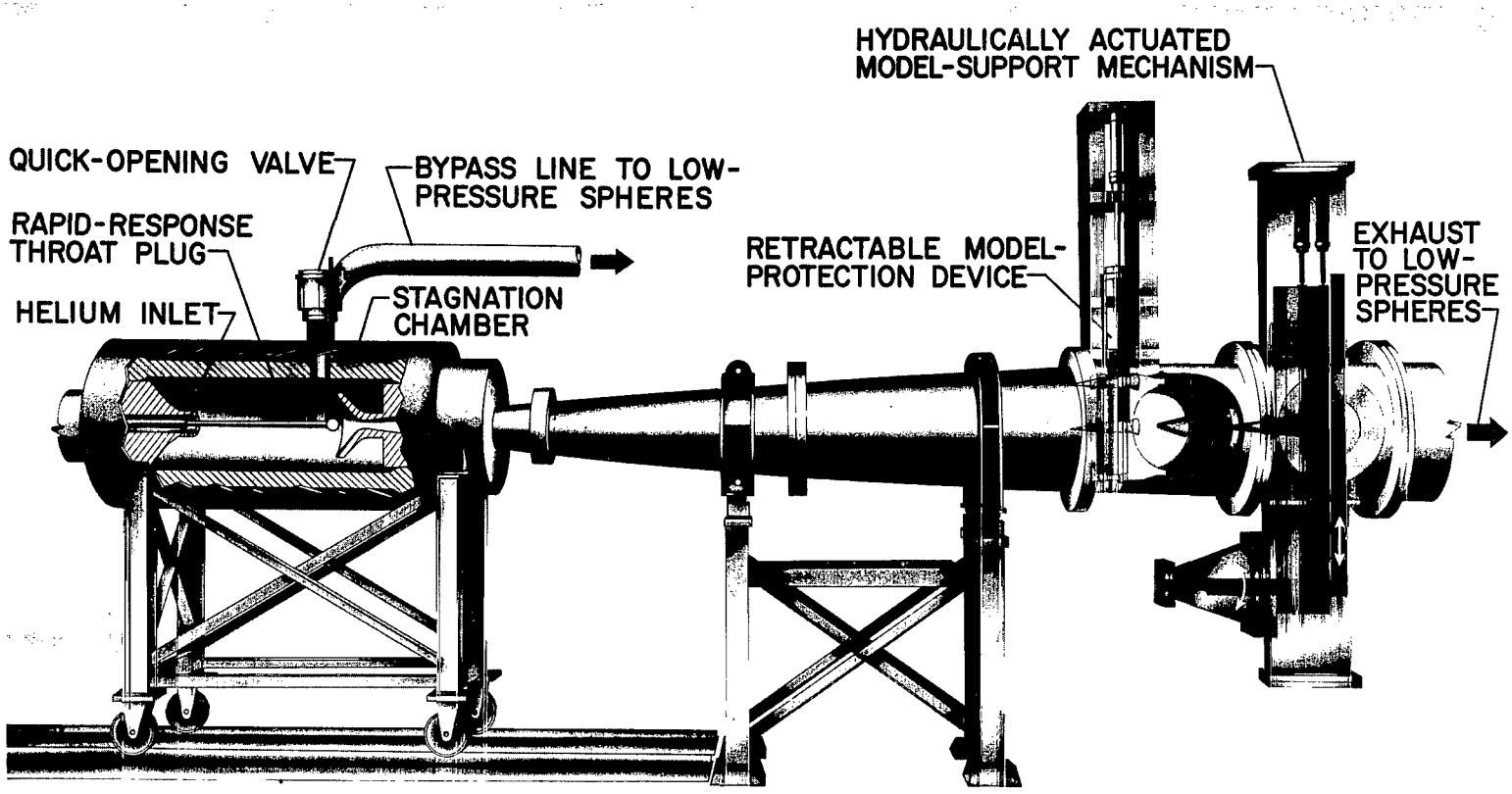

Figure 2.- Perspective drawing of Langley 22-inch helium tunnel with contoured nozzle. L-1718

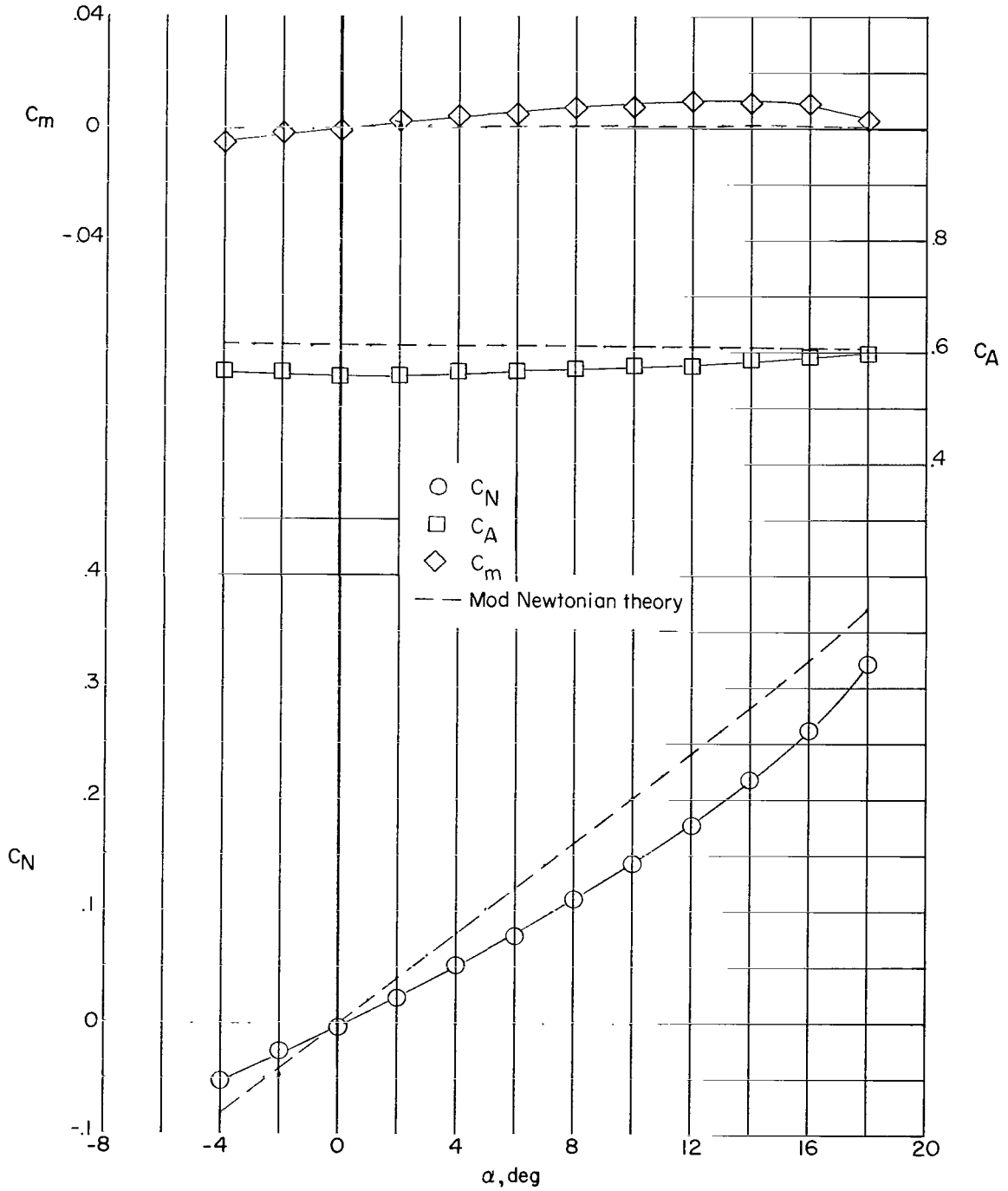

(a) $M = 19.0$; $R_D = 0.25 \times 10^6$.

Figure 3.- Longitudinal aerodynamic characteristics of R-5 reentry configuration at various Reynolds numbers.

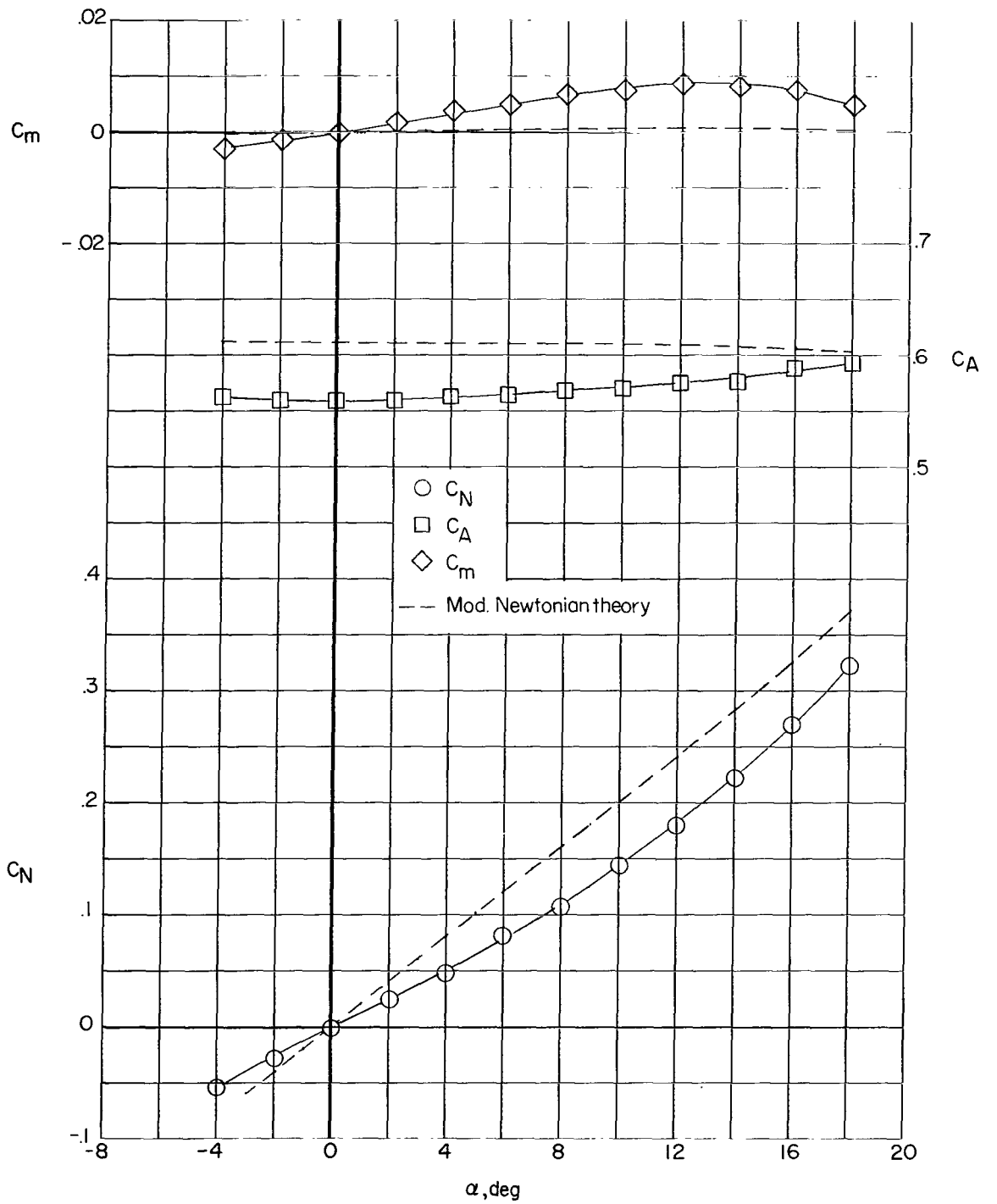

(b) M = 19.0; $R_D = 0.38 \times 10^6$.

Figure 3.- Continued.

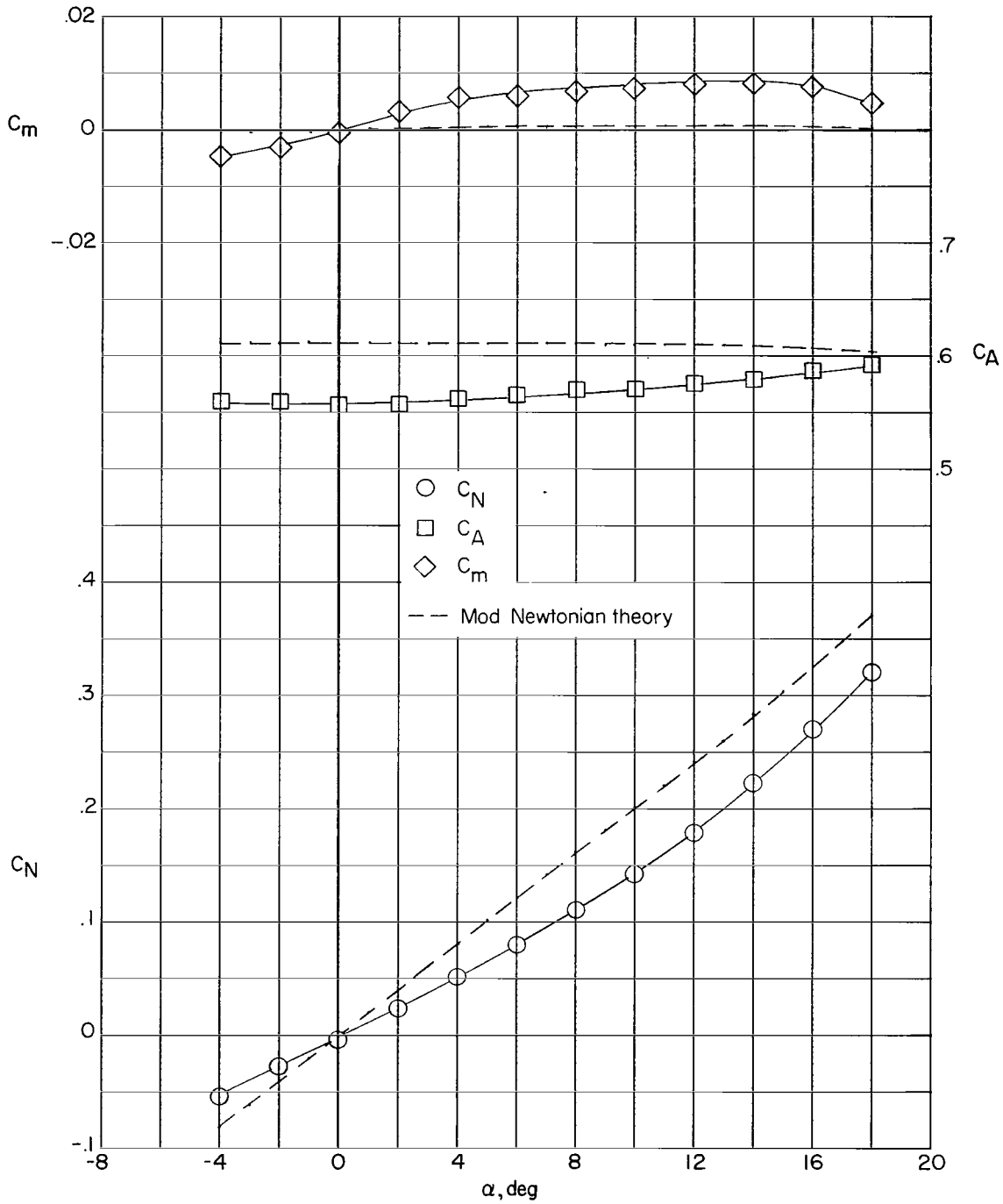

(c) M = 20.3; $R_D = 0.70 \times 10^6$.

Figure 3.- Continued.

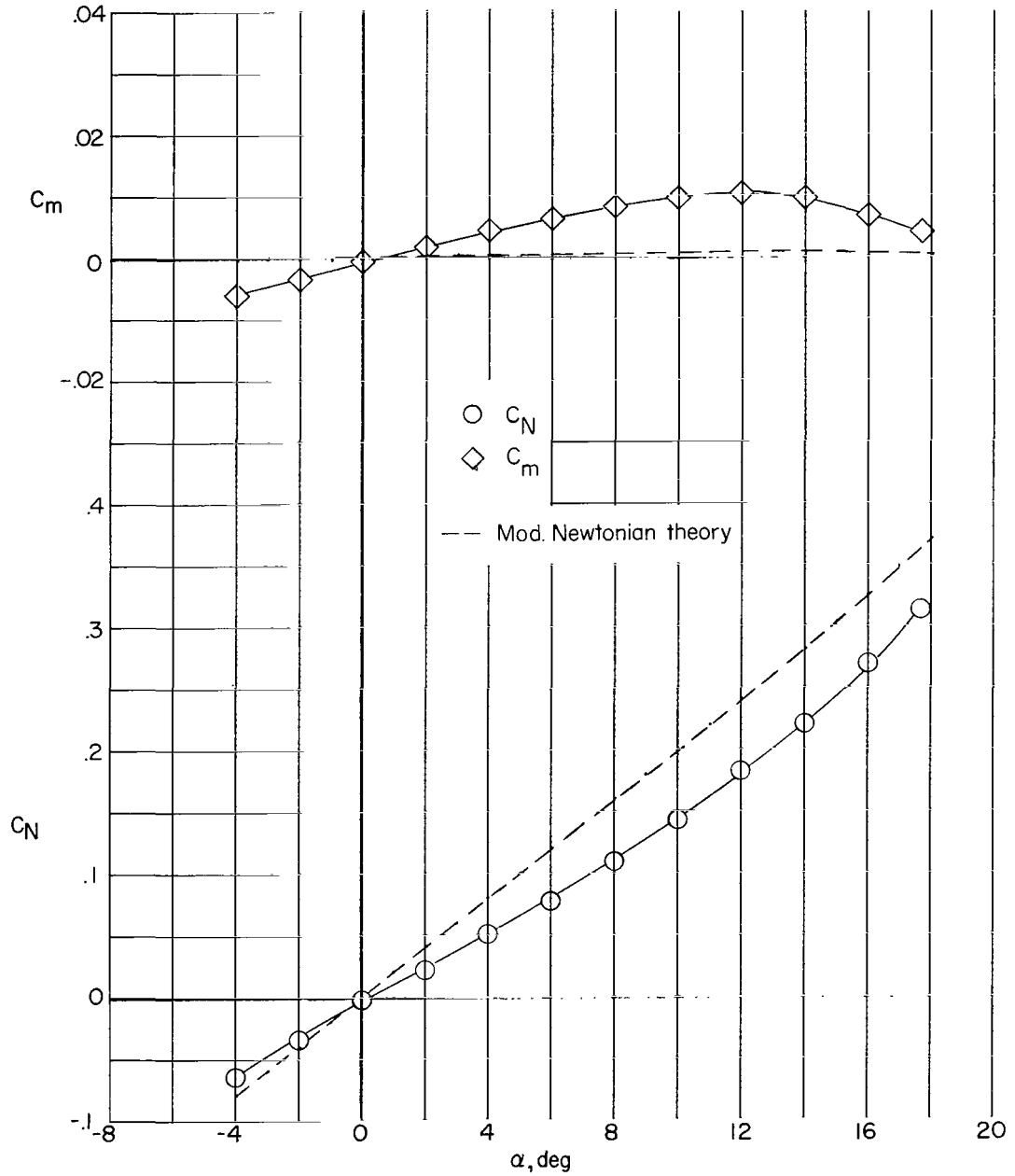

(d) M = 20.3; $R_D = 1.39 \times 10^6$.

Figure 3.- Continued.

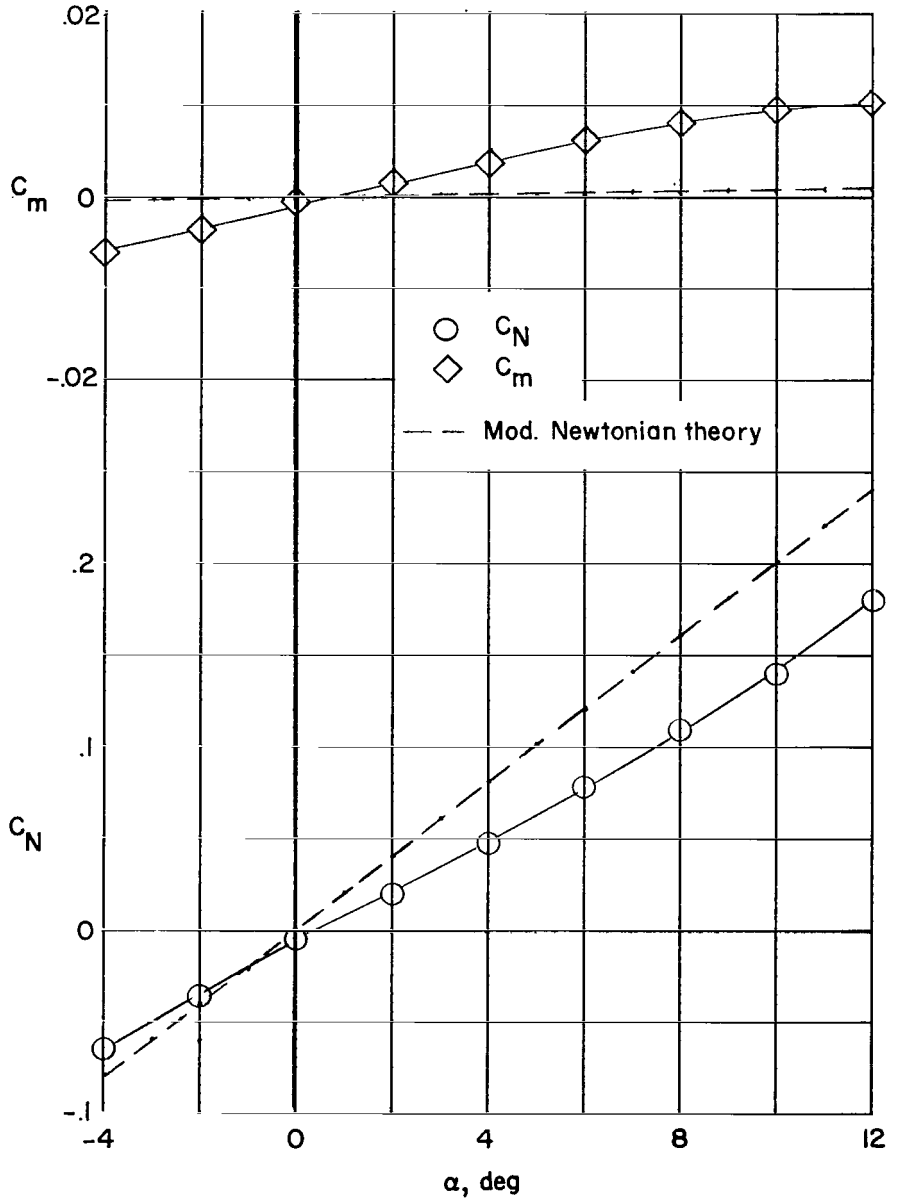

(e) $M = 21.6$; $R_D = 2.56 \times 10^6$.

Figure 3.- Continued.

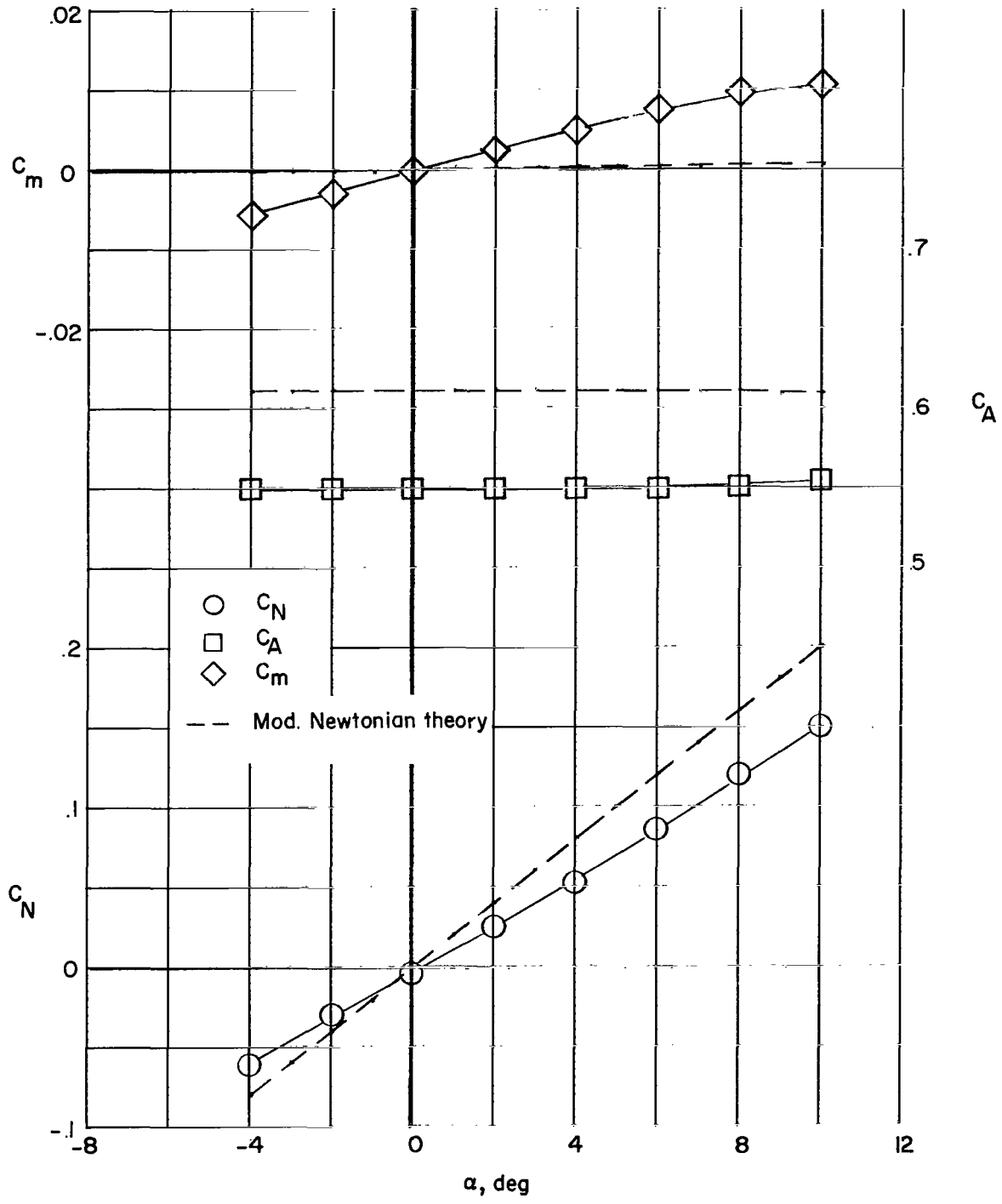

(f) $M = 21.6$; $R_D = 3.76 \times 10^6$.

Figure 3.- Concluded.

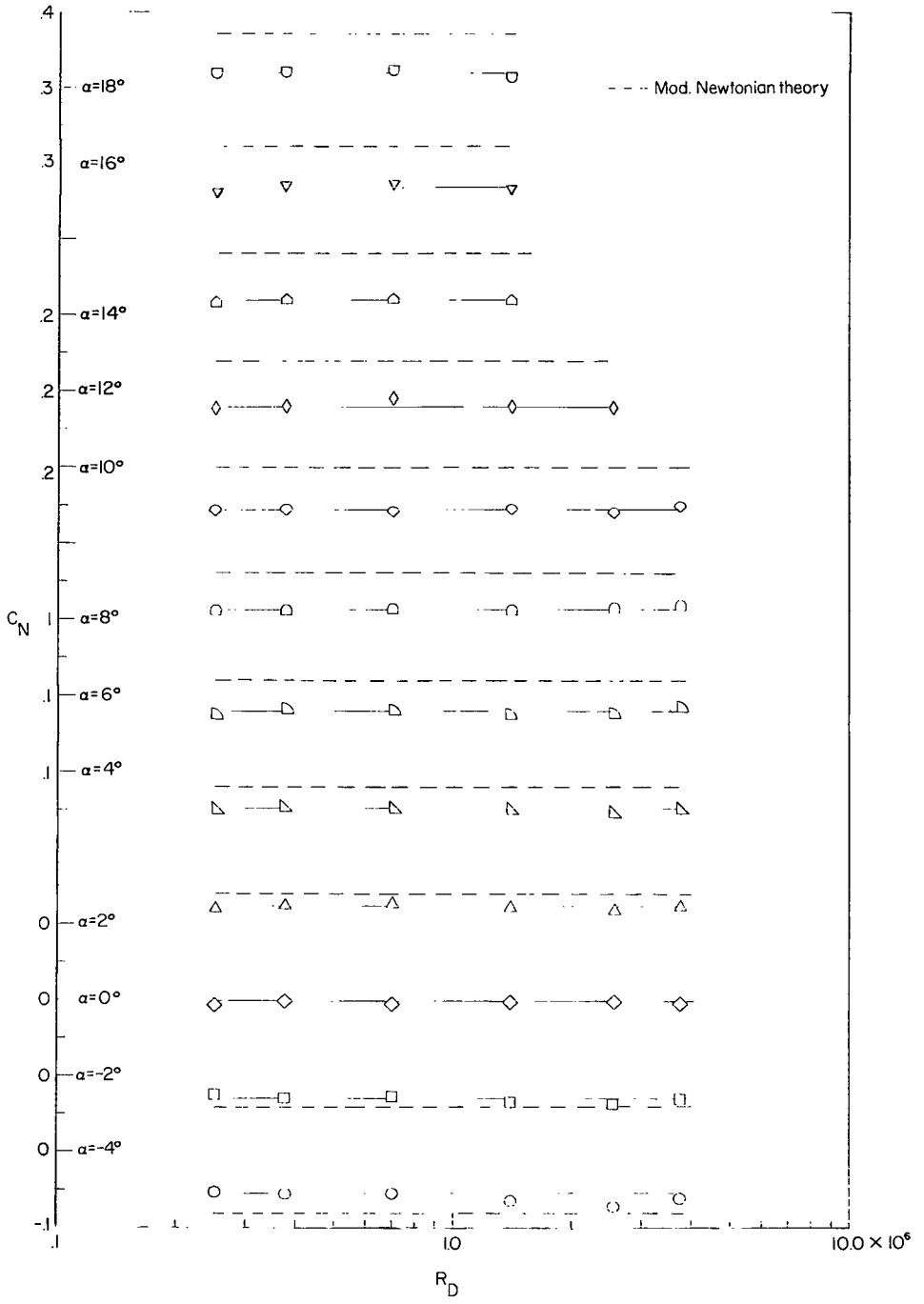

(a) Normal-force coefficient.

Figure 4.- Effect of Reynolds number and angle of attack on longitudinal aerodynamic characteristics of R-5 reentry configuration.

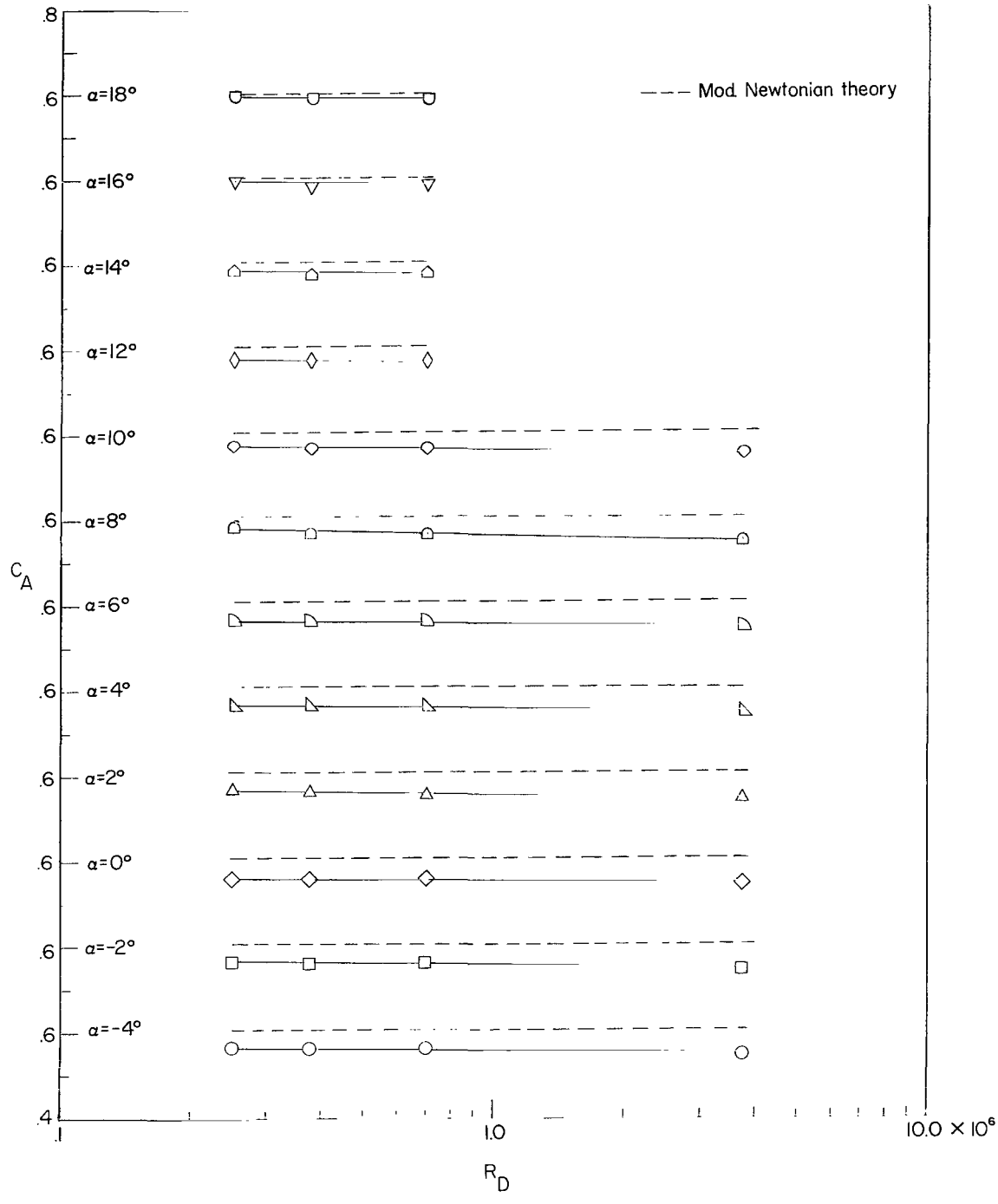

(b) Axial-force coefficient.

Figure 4.- Continued.

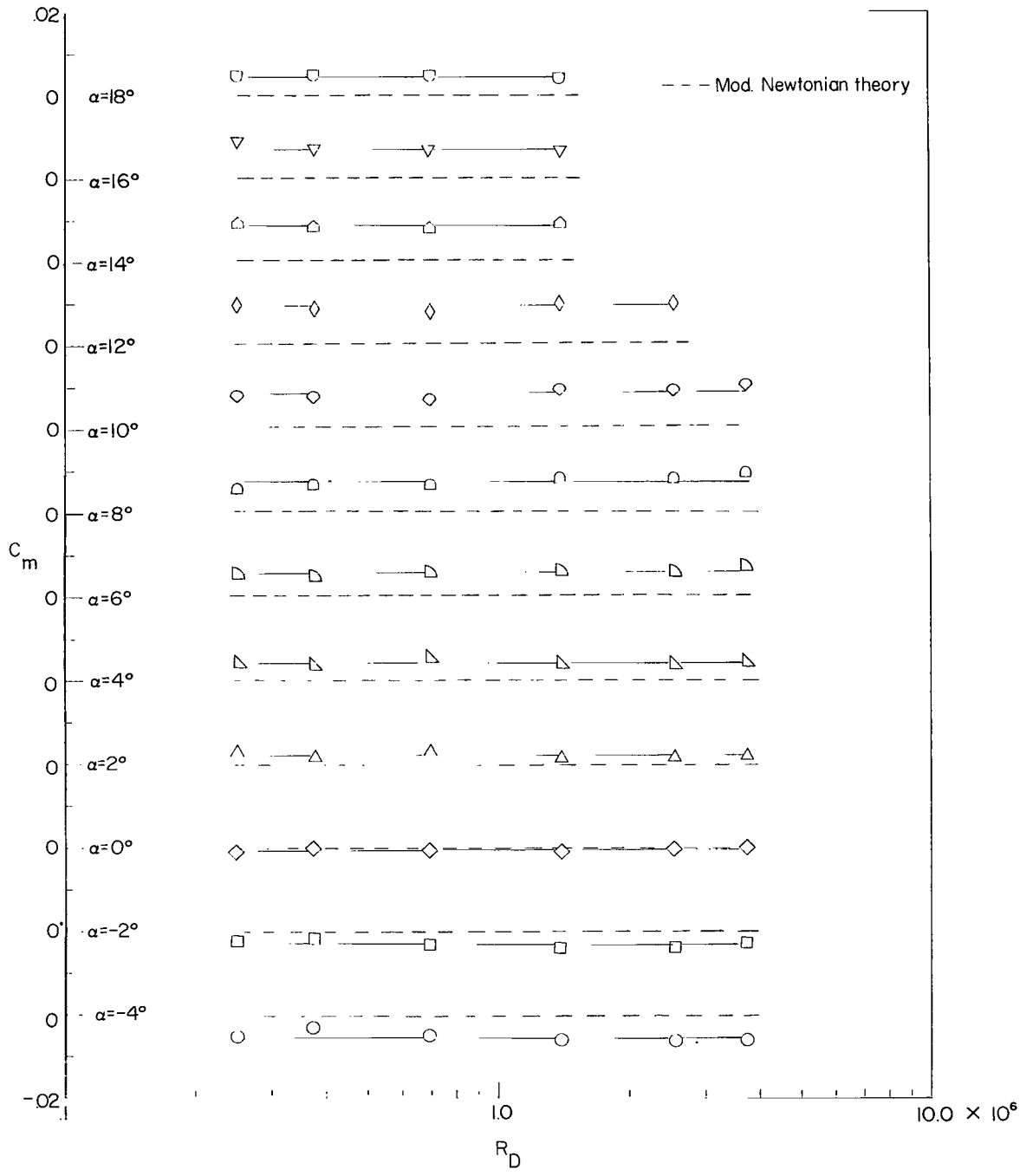

(c) Pitching-moment coefficient.

Figure 4.- Concluded.

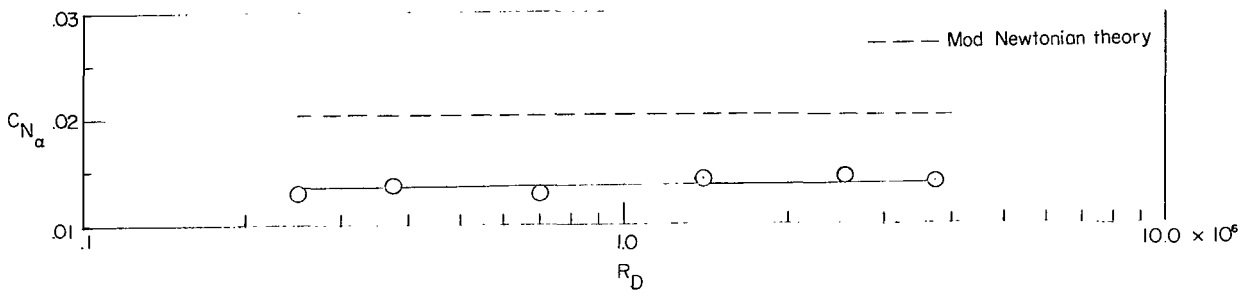

Figure 5.- Effect of Reynolds number on C_{N_α} of R-5 reentry configuration.

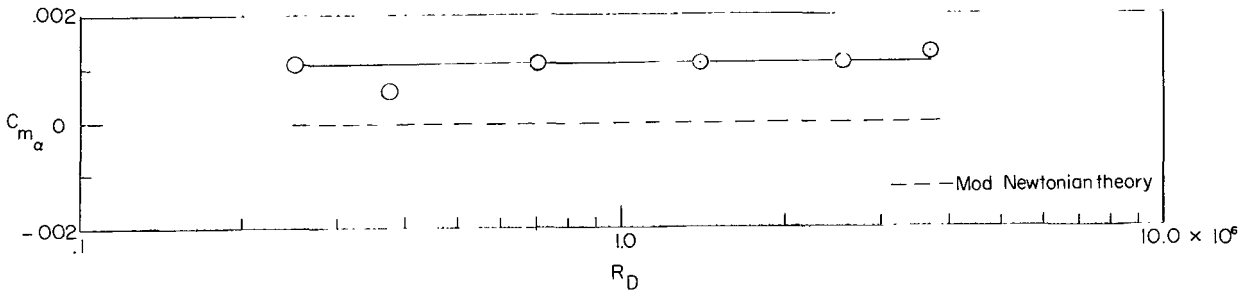

Figure 6.- Effect of Reynolds number on C_{m_α} of R-5 reentry configuration.

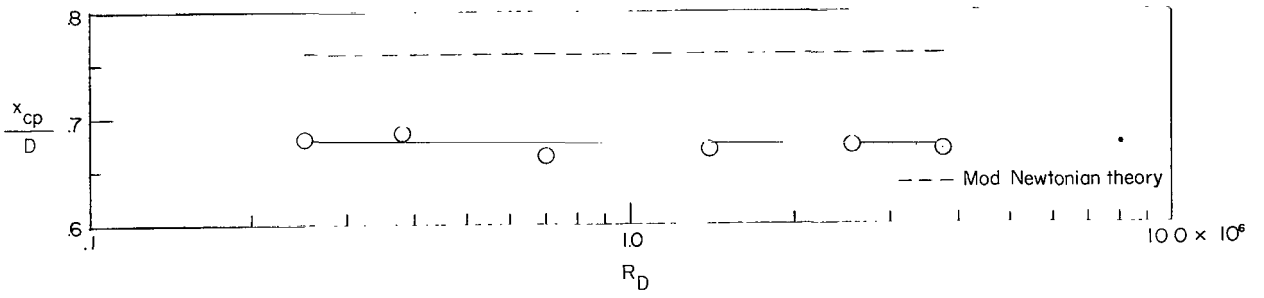

Figure 7.- Effect of Reynolds number on $\frac{x_{cp}}{D}$ of R-5 reentry configuration.

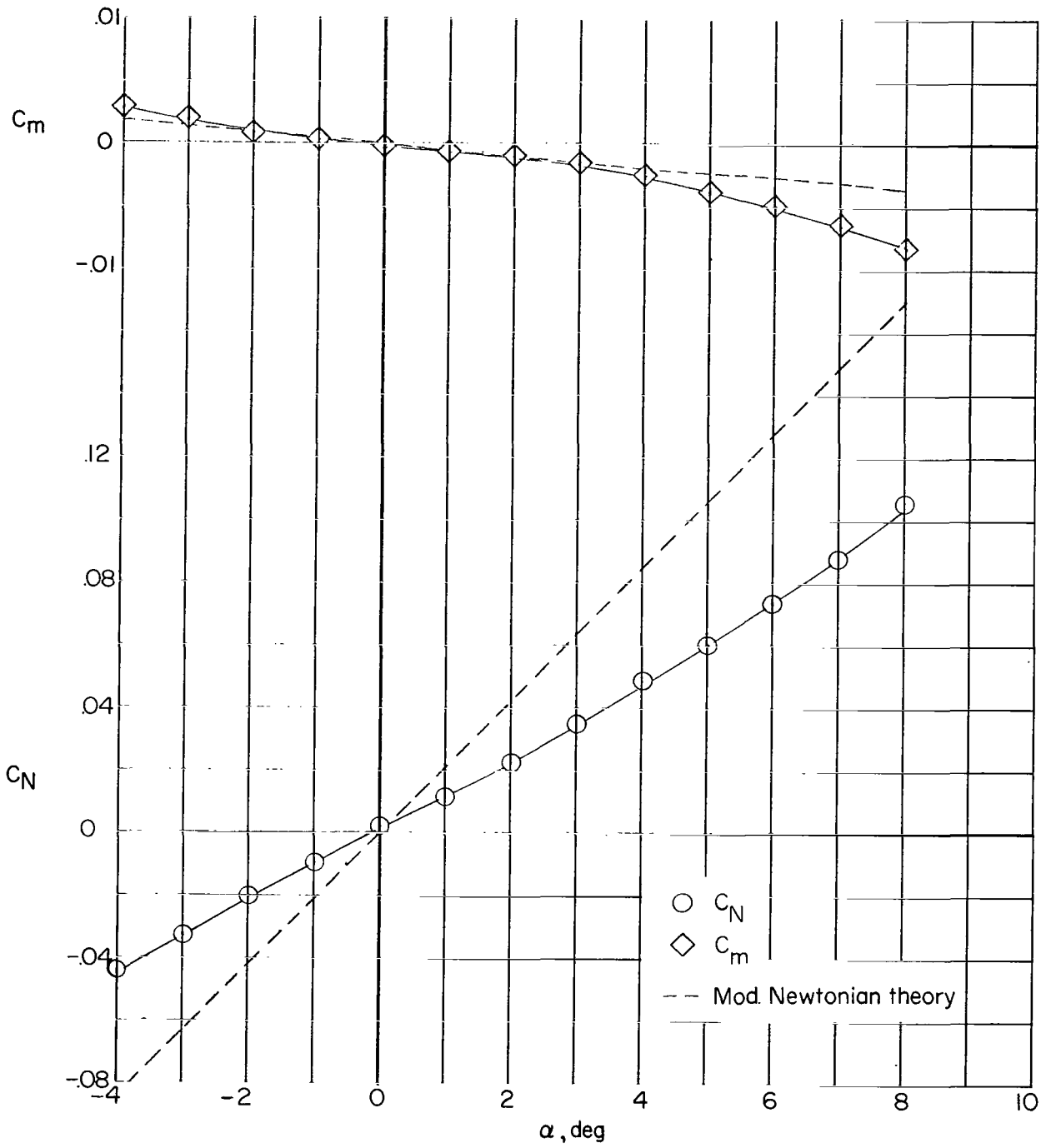

(a) $M = 19.0$; $R_D = 0.27 \times 10^6$.

Figure 8.- Longitudinal aerodynamic characteristics of N_4B_4 reentry configuration at various Reynolds numbers.

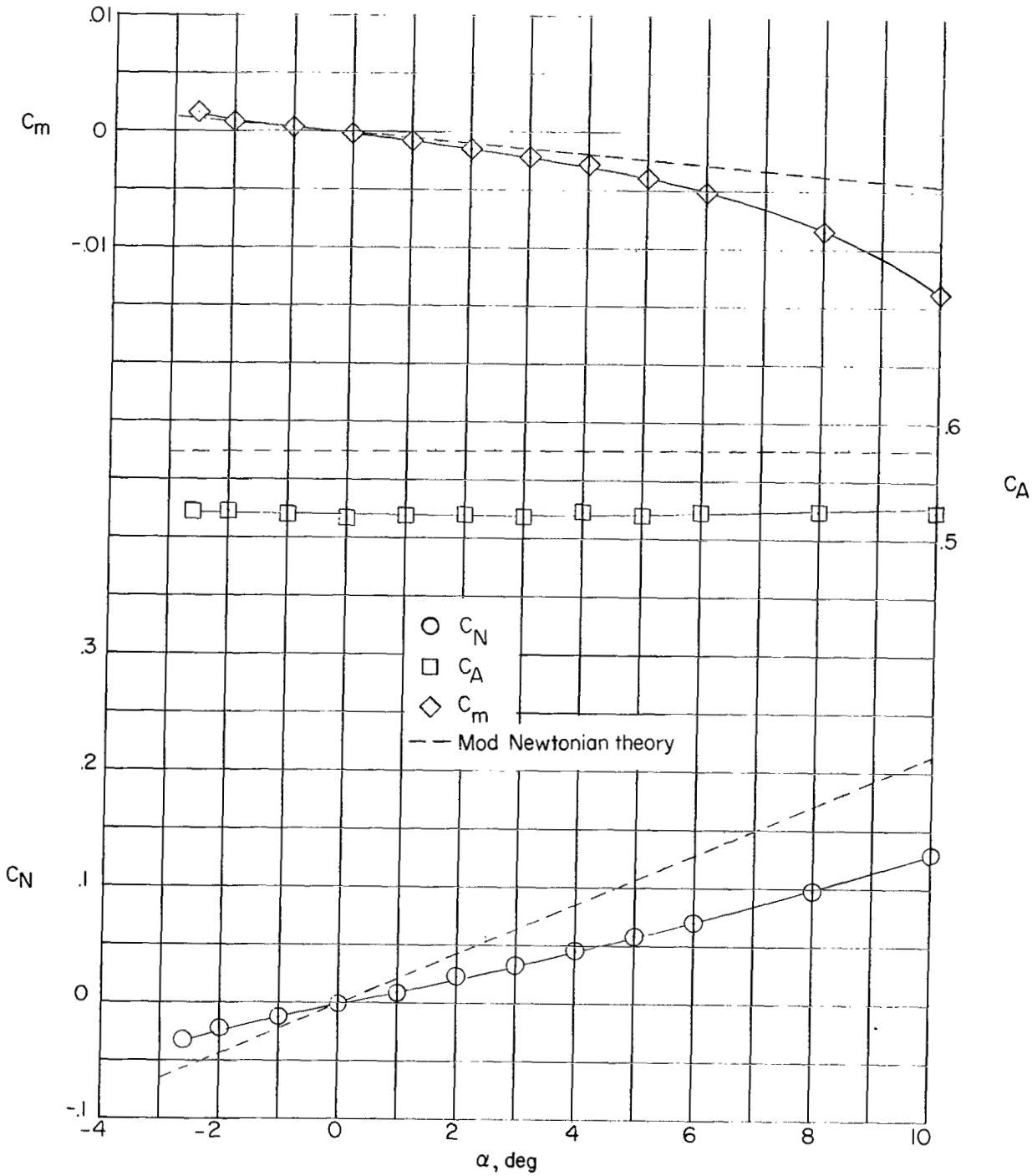

(b) M = 20.3; $R_D = 0.96 \times 10^6$.

Figure 8.- Continued.

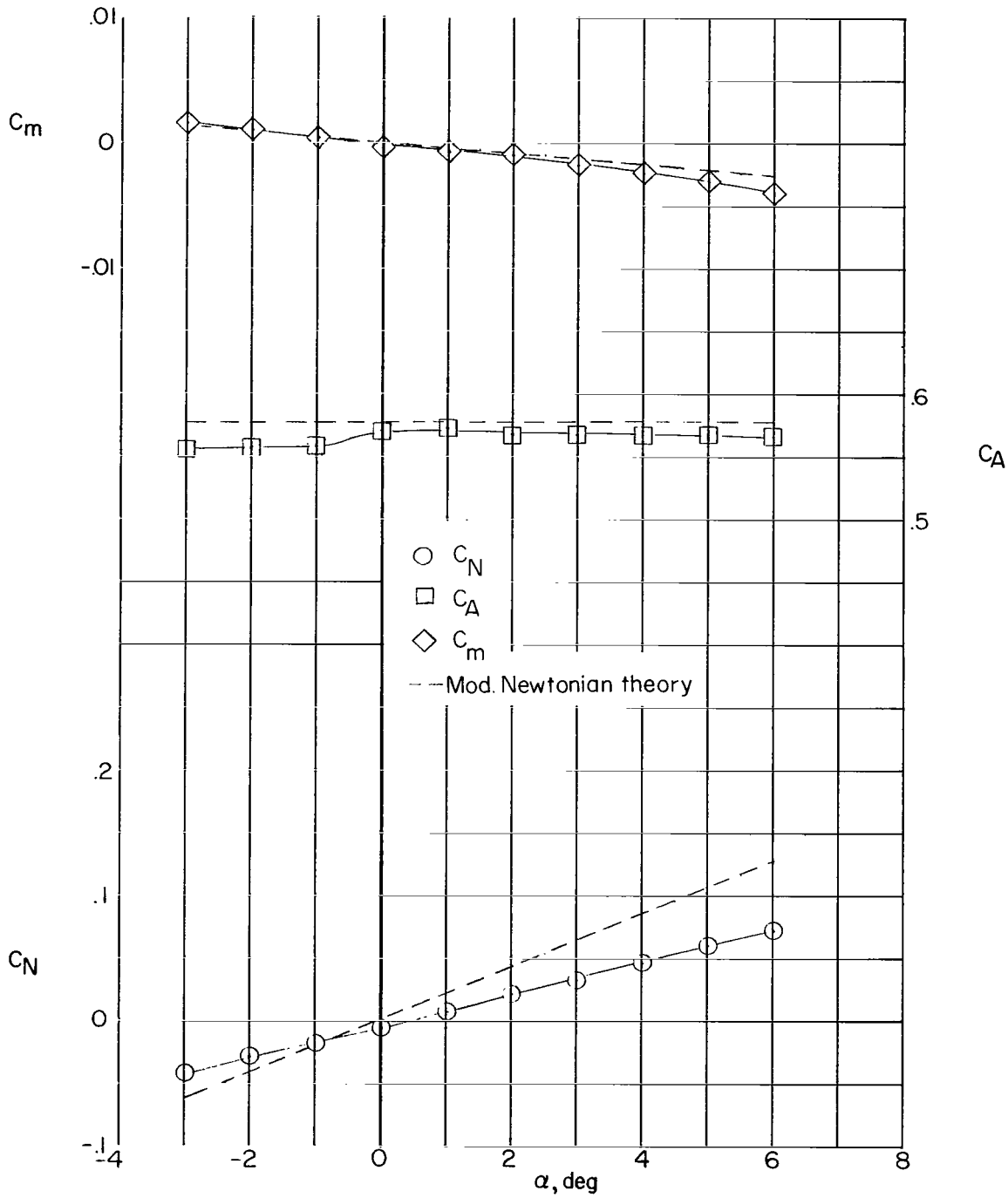

(c) M = 22.2; $R_D = 2.37 \times 10^6$.

Figure 8.- Continued.

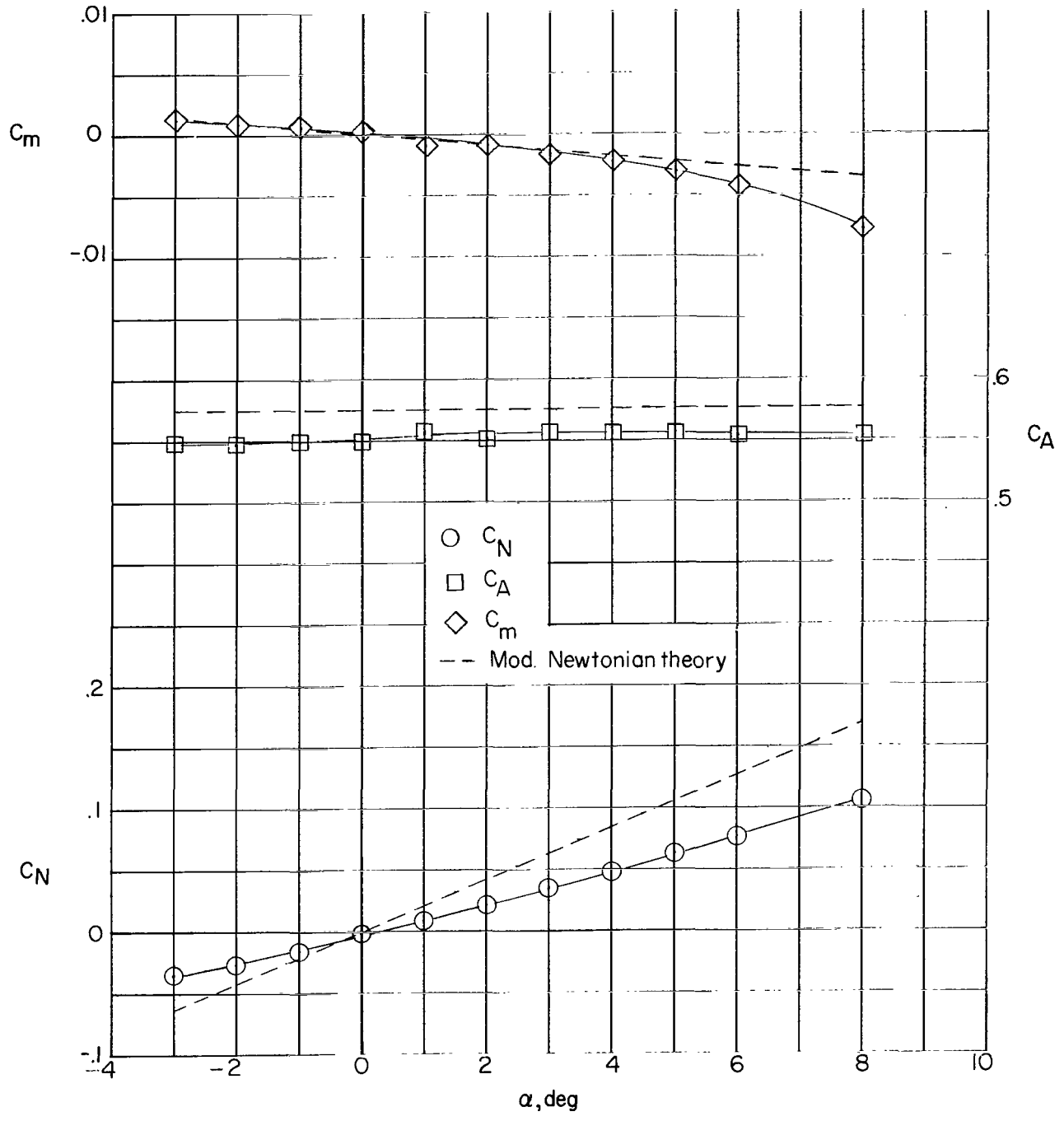

(d) $M = 21.6$; $R_D = 3.36 \times 10^6$.

Figure 8.- Concluded.

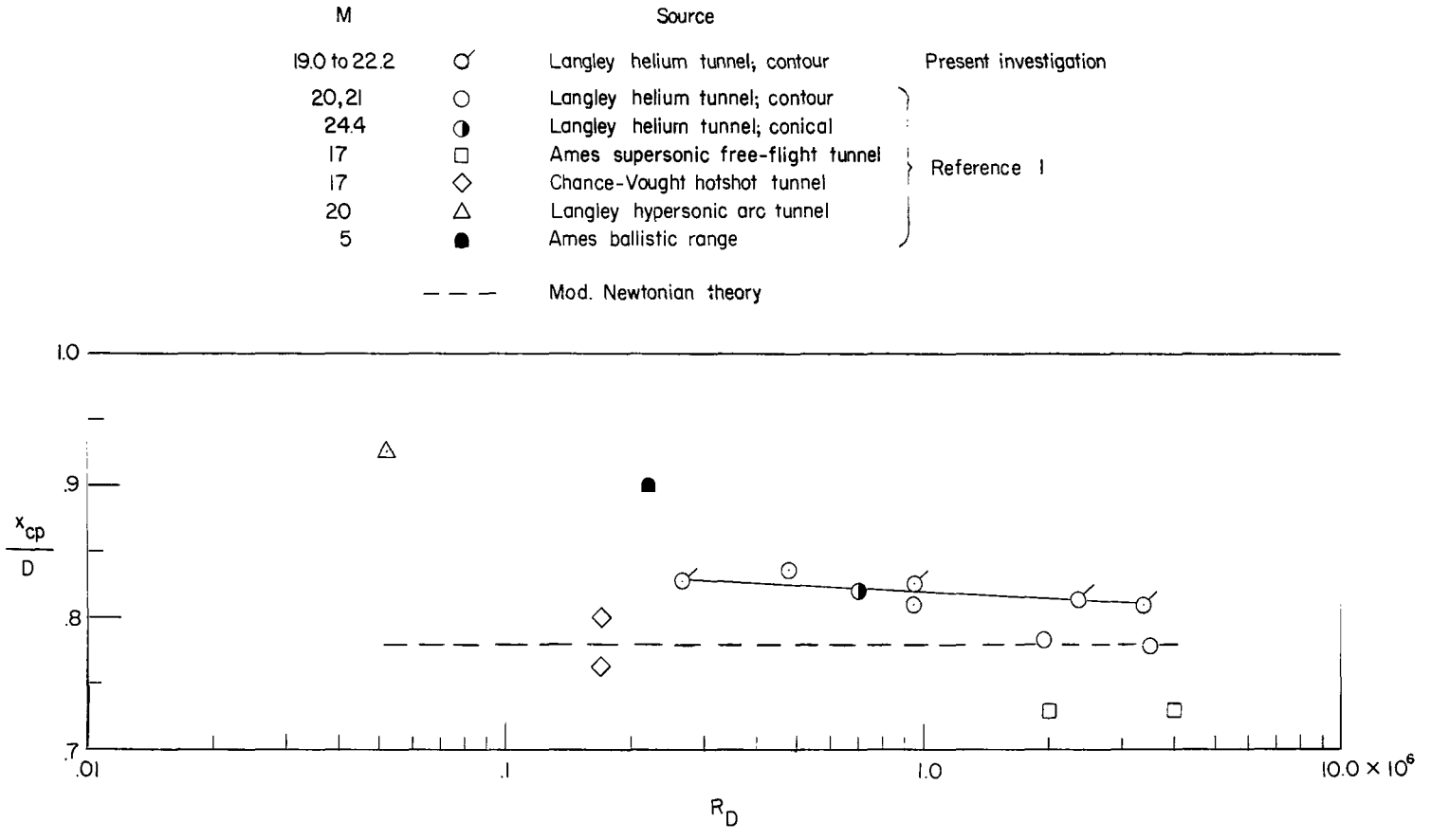

Figure 9.- Effect of Reynolds number on $\frac{x_{cp}}{D}$ of N_4B_4 reentry configuration.

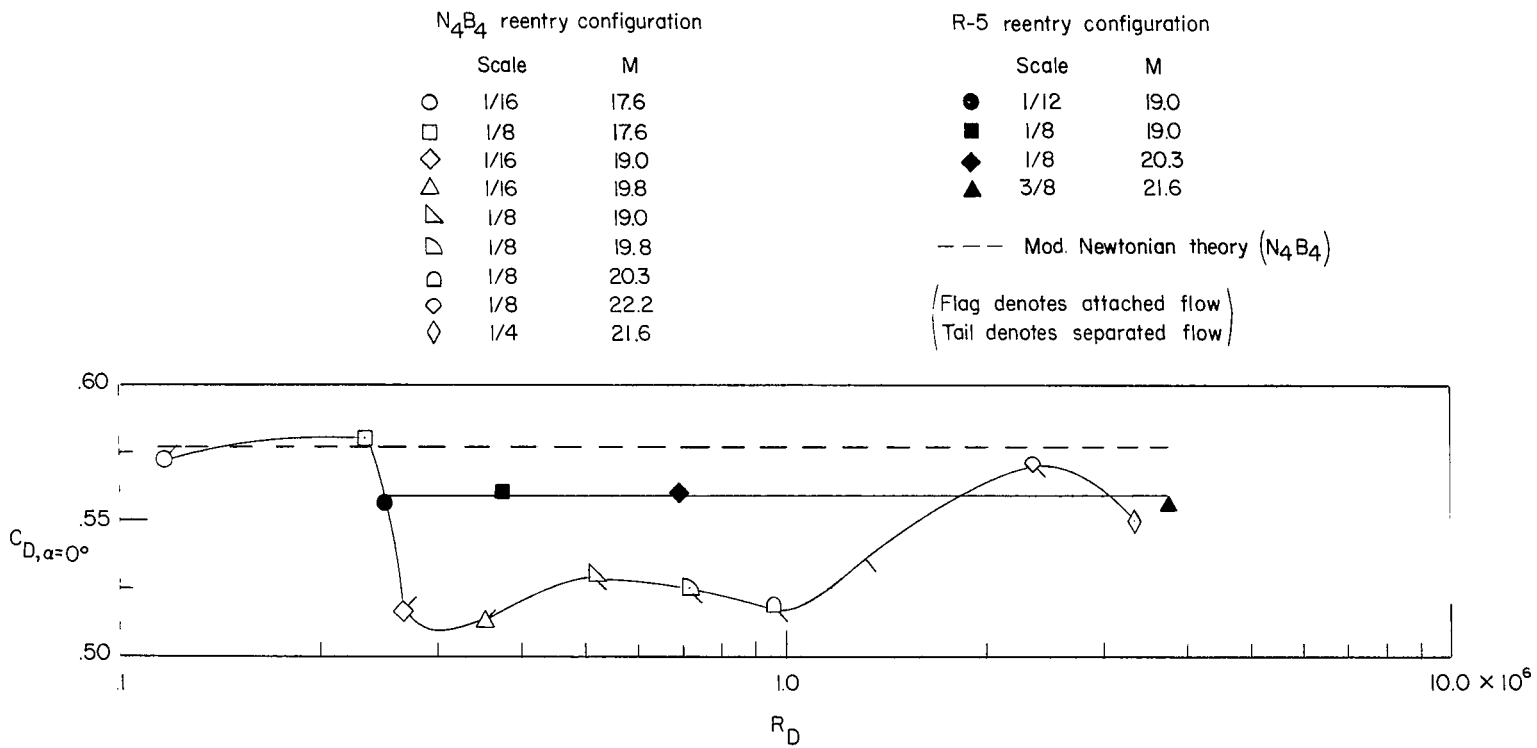

Figure 10.- Effect of Reynolds number on $C_{D,\alpha=0^o}$ of N_4B_4 and R-5 reentry configurations.

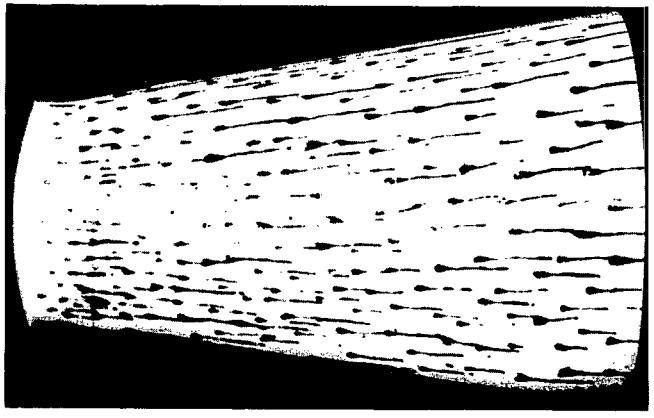

(a) M = 17.6; $R_D = 0.13 \times 10^6$.

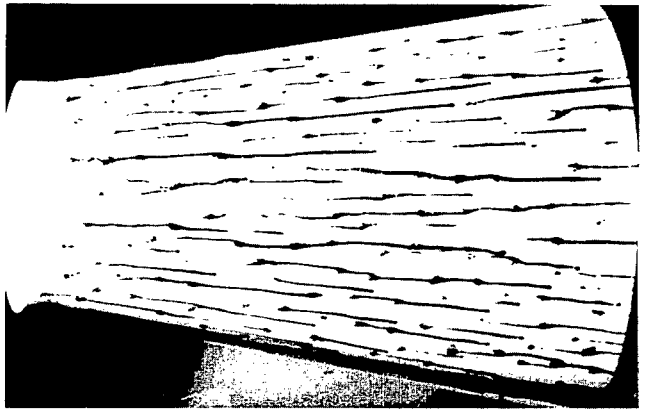

(b) M = 19.0; $R_D = 0.27 \times 10^6$.

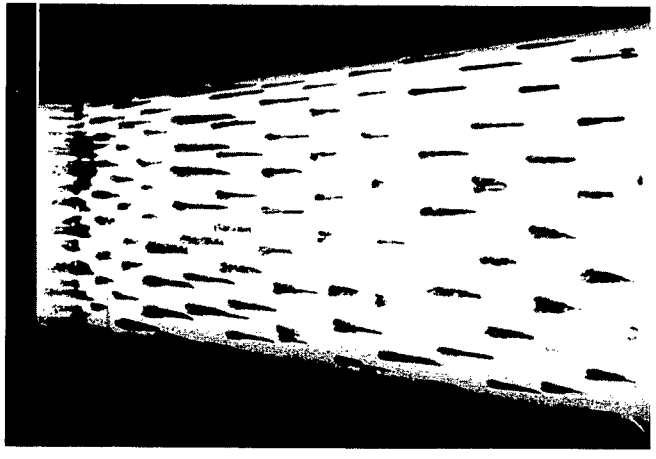

(c) M = 19.8; $R_D = 0.36 \times 10^6$.

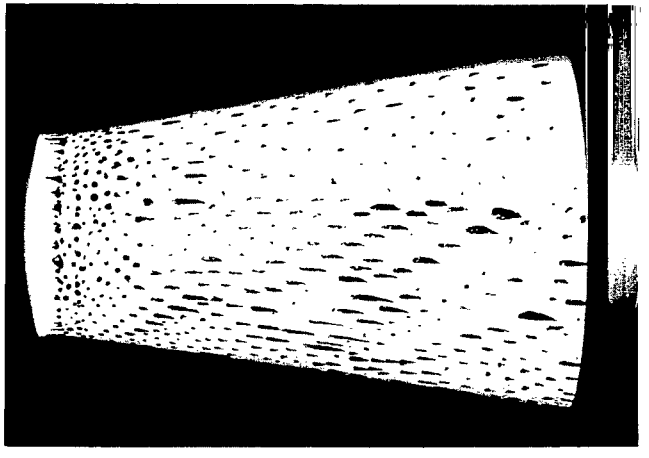

(d) M = 19.0; $R_D = 0.53 \times 10^6$.

Figure 11.- Surface flow studies of N_4B_4 reentry configuration at $\alpha = 0^o$.

L-65-162

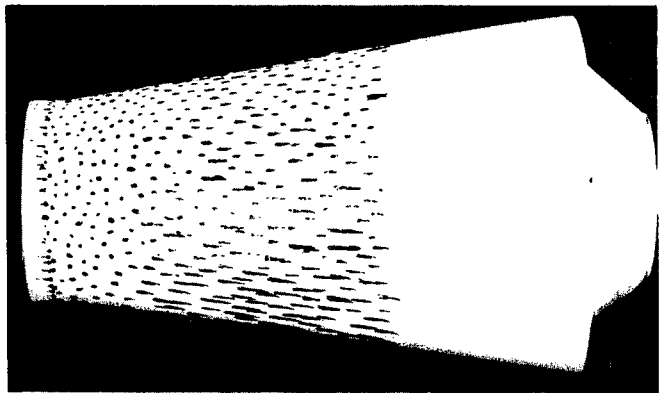

(e) $M = 19.8$; $R_D = 0.71 \times 10^6$.

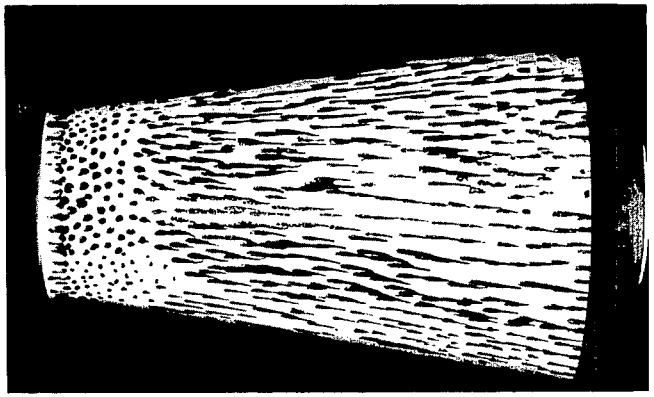

(f) $M = 20.3$; $R_D = 0.98 \times 10^6$.

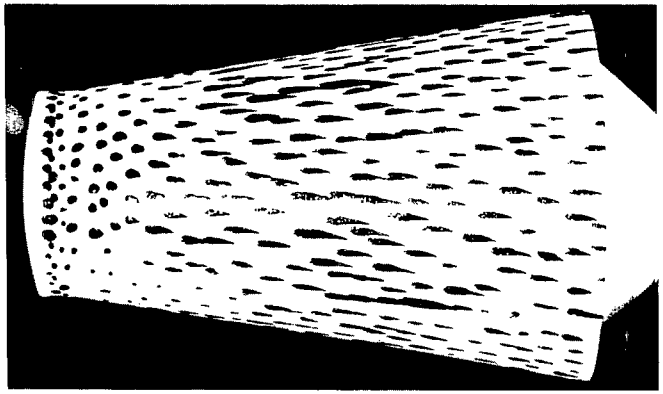

(g) $M = 21.0$; $R_D = 1.33 \times 10^6$.

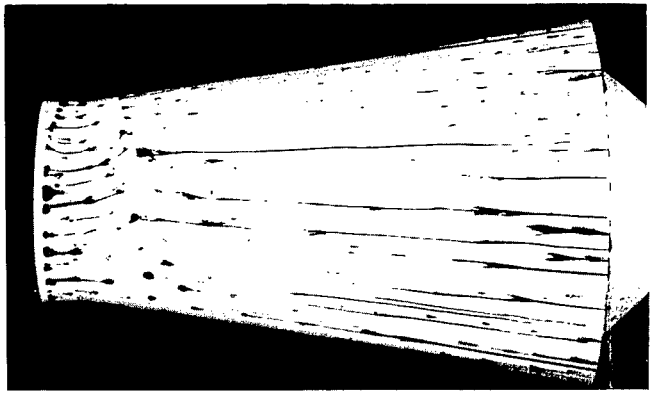

(h) $M = 22.2$; $R_D = 2.40 \times 10^6$.

Figure 11.- Concluded.

L-65-163

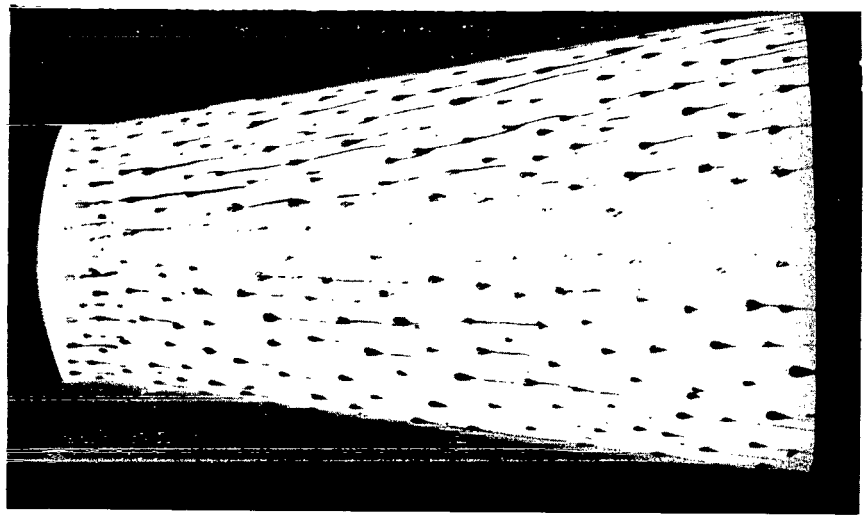

(a) $\alpha = 2^{o}$; $M = 19.0$; $R_D = 0.27 \times 10^6$. (Windward side.)

(b) $\alpha = 4^{o}$; $M = 22.2$; $R_D = 2.35 \times 10^6$. (Windward side.) L-65-164

Figure 12.- Surface flow studies on N_4B_4 reentry configuration at angles of attack greater than 0^{o}.

"The aeronautical and space activities of the United States shall be conducted so as to contribute . . . to the expansion of human knowledge of phenomena in the atmosphere and space. The Administration shall provide for the widest practicable and appropriate dissemination of information concerning its activities and the results thereof."

—NATIONAL AERONAUTICS AND SPACE ACT OF 1958

NASA SCIENTIFIC AND TECHNICAL PUBLICATIONS

TECHNICAL REPORTS: Scientific and technical information considered important, complete, and a lasting contribution to existing knowledge.

TECHNICAL NOTES: Information less broad in scope but nevertheless of importance as a contribution to existing knowledge.

TECHNICAL MEMORANDUMS: Information receiving limited distribution because of preliminary data, security classification, or other reasons.

CONTRACTOR REPORTS: Technical information generated in connection with a NASA contract or grant and released under NASA auspices.

TECHNICAL TRANSLATIONS: Information published in a foreign language considered to merit NASA distribution in English.

TECHNICAL REPRINTS: Information derived from NASA activities and initially published in the form of journal articles.

SPECIAL PUBLICATIONS: Information derived from or of value to NASA activities but not necessarily reporting the results of individual NASA-programmed scientific efforts. Publications include conference proceedings, monographs, data compilations, handbooks, sourcebooks, and special bibliographies.

Details on the availability of these publications may be obtained from:

SCIENTIFIC AND TECHNICAL INFORMATION DIVISION

NATIONAL AERONAUTICS AND SPACE ADMINISTRATION

Washington, D.C. 20546